-RESEARCH PAPER-

International Journal of Mining and Geo-Engineering

IJMGE

IJMGE 60-3 (2026) 337-346

DOI: 10.22059/IJMGE.2026.407278.595342

Advanced stability evaluation of underground marble quarry: a modelling and monitoring approach

Mritunjay Kumar [a], Akhil Avchar [a, *], and Shambhavi Sinha [a]

[a] *Department of Mining Engineering, NITK Surathkal, India.*

Article History:

Received: 10 Decemberr 2025.

Revised: 31 May 2026.

Accepted: 22 September 2026.

ABSTRACT

This study evaluated the short-to-medium term static geomechanical stability of an underground marble quarry near Gujarat, India, using an integrated geomechanical approach combining FLAC3D numerical modeling, real-time in-situ stress monitoring, and empirical methods. The room-and-pillar system in a high-strength marble rock mass (GSI=72) intersected by a dolerite dyke was analyzed across varying overburden depths (57–87 m). Modeling confirmed pillar stability with stresses of 4.15–6.87 MPa and FOS consistently above 2.0. A 2-m-thick roof layer showed localized yielding, effectively controlled by 3.5-m-long, fully grouted Fe500D rockbolts (24 mm diameter, 2.2 m×2.2 m spacing), achieving FOS of 2.27–3.93 (resin grout: 3.93). In-situ monitoring recorded stress variations of 0.2–0.4 MPa, validating predictions and enabling back-analysis that refined the deformation modulus to 35 GPa for fractured marble. Monte Carlo simulations yielded a mean pillar FOS of 2.93 (95% CI: [2.21, 3.76]), with only 0.6% probability of FOS<2.0. The validated framework confirms short-to-medium term static geomechanical stability consistent with DGMS safety requirements, supports adaptive staged excavations near the dyke, and provides a replicable model for sustainable underground dimensional stone quarrying in complex geological settings.

Keywords: *Room-and-pillar mining, Dolerite dyke, Rockbolts, In-situ monitoring, Monte Carlo simulation.*

1. Introduction

Underground quarrying of dimensional stones like marble has become a key alternative to open-pit mining due to thick overburden, strict environmental regulations, and urban proximity [1]. This approach ensures access to premium deposits while reducing surface impact and prioritizing safety [2]. With the global dimensional stone market expanding rapidly, India's marble sector, especially in Rajasthan, plays a major role [3, 4]. The Mine A underground marble quarry near, Gujarat (Figure 1) exemplifies this trend, requiring robust stability assessments to prevent geomechanical failures such as spalling or shear that can endanger lives and disrupt production [5, 6].

Stability evaluation of underground dimensional stone quarries presents complex challenges, particularly during the shift from surface to subsurface extraction under varying overburden and regulatory constraints. At Mine A, the room-and-pillar system operates in a compact white marble rock mass (GSI=72) with minimal closed fractures, complicated by a heterogeneous dolerite dyke that alters local stress fields. Key concerns include pillar stresses of 4.15–6.87 MPa, shear and tensile yielding in a 2-m-thick roof layer, and stress redistribution under overburden depths of 57–87 m, all while meeting Directorate General of Mines Safety (DGMS) standards [7, 8].

This study assesses the stability of Mine A using an integrated methodology combining FLAC3D numerical modeling, in-situ stress monitoring, and empirical analyses. The objectives are to (1) quantify stress–strain behavior, (2) validate predictions with field data, and (3) design DGMS-compliant reinforcement strategies [9].

The novelty lies in applying this framework to a non-European setting with unique features: irregular dolerite dyke boundaries, compact marble with sparse fractures, and variable overburden. Unlike earlier studies focused on highly jointed Italian quarries [12, 13], this work validates pillar FOS>2.0 and mitigates roof yielding using 3.5-m fully grouted Fe500D rockbolts (24 mm diameter, 2.2 m×2.2 m spacing), achieving FOS of 2.27–3.93. Real-time 2024 stress data (0.2–0.4 MPa variations) enabled back-analysis, refining the deformation modulus to 35 GPa and guiding adaptive staged excavations near the dyke. These site-specific insights, supported by Monte Carlo uncertainty analysis, extend global geomechanical knowledge and offer a replicable model for sustainable quarrying in complex environments.

Effective stability management integrates geological characterisation, numerical modelling (FLAC3D [15, 17]), and real-time monitoring [10, 11, 18]. Studies in Italy's Apuan Alps and Carrara demonstrate the utility of these combined methods [12, 13]. In India, FLAC3D has been applied to pillar stability in the Gujarat marble quarry [23], while multi-level stone mines have been analyzed for interburden and offset effects [24]. Established pillar strength formulas and engineering classifications provide additional rigor [14, 25, 26]. This study builds on these foundations, delivering practical, data-driven solutions for safe and sustainable underground marble extraction. Figure 1 shows the opencast pit of Mine A marble quarry.

2. Geological characterisation

The Mine A underground marble quarry, located near in the Banaskantha district of Gujarat, India in proximity to the Gujarat–Rajasthan border exploits a high-quality white marble deposit within a structurally controlled formation hosted by gneissic and quartzitic rocks. Systematic field mapping reveals a compact rock mass with

* Corresponding author: *E-mail address:* akhil@nitk.edu.in (A. Avchar).

predominant ENE-WSW fracture orientation, which strongly influences underground stability and excavation strategy.

Detailed field surveys conducted revealed a rock mass with infrequent discontinuities, predominantly closed and devoid of water circulation, thereby minimizing the potential for wedge detachment or localized instability (Figure 2). The observed fractures are micro-scale cracks with planar morphology, rough surfaces, and minimal persistence (10–20 mm), as per ISRM standards (ISRM, 1978). These cracks, distinct from major structural discontinuities, have apertures of 0.1–0.5 mm and minimally influence wedge formation but contribute to local shear resistance (JRC=12–16, Table 2). These characteristics align with the findings of Oggeri and Oreste (2015) at the Candoglia cavern, where a low joint density contributed to sustained short-to-medium term static stability, albeit with vigilance for rigid wedge movements.

A prominent geological feature in Mine A is a dolerite dyke in Room 4, as visible in the underground working (Figure 3). The dyke exhibits irregular, diffuse boundaries with host marble—unlike its defined 3-m-wide appearance in the prior open-pit. This suggests intrusion into semi-plastic carbonate sediment, creating a heterogeneous rock mass with intermixed compositions confirmed by Room 4 sample analyses. This required conservative rock mass characterization using average properties to address reduced structural coherence.

Figure 1. View of the opencast pit of Mine A marble quarry.

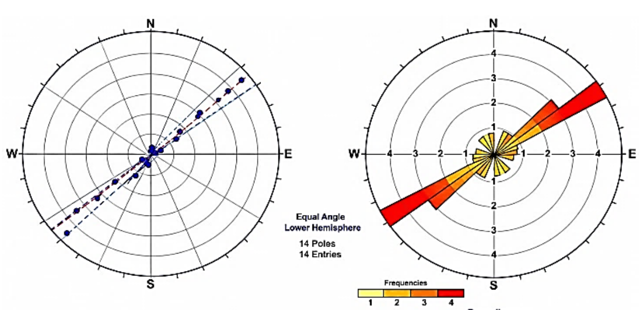

Figure 2. Fracture orientation in the Mine A quarry, illustrating the ENE-WSW trend of discontinuities.

Laboratory tests on intact marble yielded UCS=53.3 MPa, Young's modulus=63.7 GPa, density=2880 kg/m³, low imbibition (0.064%), and high Knoop hardness (1382 MPa), confirming its competence for dimensional stone extraction (Table 1).

Field rock mass characterization employed GSI, RMR, and Barton-Bandis JRC parameters. The marble was classified into two types: intact (GSI=100, RMR=100) and scattered fractured (GSI=72, RMR=75), the latter dominant. Fractured zones feature discontinuities spaced>2 m, with rough planar surfaces (JRC=12–16), dry, unweathered, and unfilled, providing good shear resistance. Both types fall under excavation category C (ESR=1.2–1.6) per Barton (1995), suitable for undisturbed quarrying.

The mechanical properties of Mine A's white marble rock mass were derived using the Hoek-Brown criterion (Hoek et al., 2002 [5]; Table 3), illustrated in Figure 4, and deformation modulus estimates (Hoek and Diederichs, 2006; Table 3) via RockLab software. Intact rock mass exhibited global strength (σ_cm)=49.3 MPa, cohesion=11.0 MPa, and friction angle=41.8°. The dominant scattered fractured rock mass showed reduced values: σ_cm=15.3 MPa, cohesion=3.9 MPa, and friction angle=35.9°, reflecting discontinuity effects. Deformation modulus was 45 GPa (intact) and 35 GPa (fractured), indicating adequate stiffness for underground workings but necessitating careful stability management (Oggeri & Oreste, 2015).

Figure 3. View of the underground room showing dolerite dyke contact zone, Room 4.

Table 1. Physical and Mechanical Characteristics of White Marble (Mine A).

Material Property	Value	Unit
Specific mass	2.88	g/cm³
Water absorption coefficient	0.064	%
Compressive strength (uniaxial)	533	bar
Flexural strength	8.8	MPa
Elastic modulus	63.69	GPa
Poisson's ratio	0.308	–
Abrasion loss (thickness)	0.69	cm
Impact resistance height	360	mm
Thermal expansion coefficient	8.8	10^{-6}/°C
Microhardness (Knoop)	1382	MPa

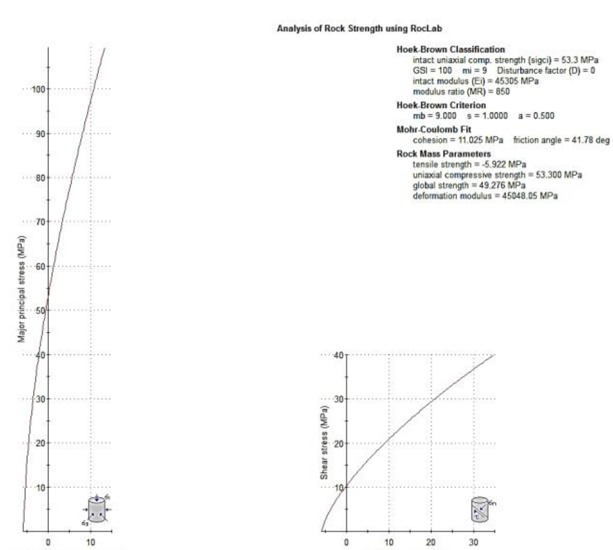

Figure 4. Hoek & Brown failure criterion for intact rock-mass of the Mine A Marble.

Table 2. Geomechanical input data for Marble Mine A.

Property	Unit	Intact Rock-Mass	Scattered Fractured Rock-Mass
Compressive strength (uniaxial)	MPa	53.3	53.3
Specific mass	g/cm³	2.88	2.88
Hoek-Brown material constant (m_i)	–	9	9
Rock Quality Designation (RQD)	%	100	83.5
Spacing of discontinuities	m	–	>2
Aperture of discontinuities	mm	–	0.1–0.5
Persistency of discontinuities	mm	–	10–20
Roughness of discontinuities	–	12-16	Rough
Morphology of discontinuities	–	–	Planar

Table 3. Mine A Marble rock mass mechanical property values.

Property	Unit	Intact Rock-Mass	Scattered Fractured Rock-Mass
Rock Mass Rating (RMR)	–	95	75
Geological Strength Index (GSI)	–	100	72
Modulus Ratio (MR)	–	850	850
Intact Rock Modulus (E_i)	GPa	45.305	45.305
Hoek-Brown Parameter (m_β)	–	9	3.31
Hoek-Brown Parameter (s)	–	1	0.045
Hoek-Brown Parameter (a)	–	0.5	0.502
Cohesion of Rock Mass	MPa	11.0	4
Friction Angle of Rock Mass	°	41.8	36
Uniaxial Compressive Strength (σc)	MPa	53.300	11.35
Global Strength of Rock Mass (σcm)	MPa	49.276	14.9
Tensile Strength of Rock Mass (σt)	MPa	-5.922	-0.719
Deformation Modulus (E_{xx})	GPa	45.048	36

This comprehensive characterization establishes a robust foundation for stability assessments, integrating field observations, laboratory data, and empirical classifications. The compact nature of the Mine A marble, its minimal fracturing, and the nuanced influence of the dolerite dyke collectively necessitate the zoned numerical modelling approach adopted in section 3.1.

3. Methodology

The stability assessment of the Mine A underground marble quarry was conducted through an integrated approach combining numerical modeling, in-situ monitoring, and empirical formulations. This multi-faceted strategy aimed to evaluate the stress-strain behavior of the rock mass, validate design assumptions, and ensure compliance with safety standards set by the Directorate General of Mines Safety (DGMS). The methodology encompassed three primary components: numerical modeling to simulate excavation phases, monitoring systems to capture real-time rock mass responses, and empirical analyses to estimate pillar stability, each detailed below.

3.1. Numerical modeling

Numerical modeling was performed using FLAC3D (Itasca Consulting Group), a finite-difference code widely adopted for geomechanical analyses in underground excavations due to its ability to simulate complex stress distributions and plastic behavior (Oggeri & Oreste, 2015). The model focused on the room-and-pillar system at an elevation of 365 meters above sea level (mSL), representing the primary horizon of underground workings at Mine A (Figure 8). The model incorporated site-specific pillar dimensions (Table 4) and geomechanical properties of the marble rock mass, derived from laboratory and field characterizations (Tables 2 and 3).

The model geometry was constructed based on detailed mine surveys, including the complete mine map (Figure 5), underground workings layout (Figure 6), and a critical cross-section (D1-D2) of the quarry site (Figure 7). These spatial data ensured accurate representation of the quarry's configuration, with pillars designed as thick elements (minimum side dimension at least twice the height) to enhance stability. The excavation sequence was simulated in three distinct steps to reflect the planned mining progression:

1. Enlargement of Area 1: Initial lateral expansion of the Room in Area 1, increasing the void span while maintaining existing pillars.
2. Downward Excavation in Area 1: A vertical deepening of 5.5 meters below the floor of Area 1, simulating benching operations.
3. Area 2 Enlargement and Further Deepening: Lateral expansion of Area 2, coupled with an additional 11-meter vertical excavation below the floors of both Areas 1 and 2, representing progressive mining advancement.

Table 4. Size of the pillars.

Pillar	Side A [m]	Side B [m]
Pillar 1	30	12
Pillar 2	82	12
Pillar 3	32	12
Pillar 4	30	18
Pillar 5	30	12
Pillar 6	40	12
Pillar 7	32	24

All numerical analyses stress distribution, plasticity state assessment, Factor of Safety computation via strength reduction, and rockbolt reinforcement simulation were performed entirely within FLAC3D Version 6.0 (Itasca Consulting Group, 2017 [15]). Prior to model construction, Hoek-Brown parameters (Table 3) were converted to equivalent Mohr-Coulomb parameters using RockLab software, applying the generalised Hoek-Brown criterion (Hoek et al., 2002 [5]) across the stress range appropriate to Mine A overburden depths of 57-87 m. The integrated workflow comprised: (1) field characterisation and laboratory testing; (2) GSI and RMR classification; (3) Hoek-Brown parameter derivation via RockLab; (4) Mohr-Coulomb conversion for FLAC3D zone assignment (intact marble: c=11.0 MPa, phi=41.8 deg; fractured marble: c=3.9 MPa, phi=35.9 deg); (5) staged excavation simulation; (6) Factor of Safety via strength reduction; and (7) back-analysis to match monitored stress data. The dolerite dyke was treated using a conservative equivalent-continuum approach with lower-bound fractured marble parameters. This limitation is acknowledged in Section 4.4.

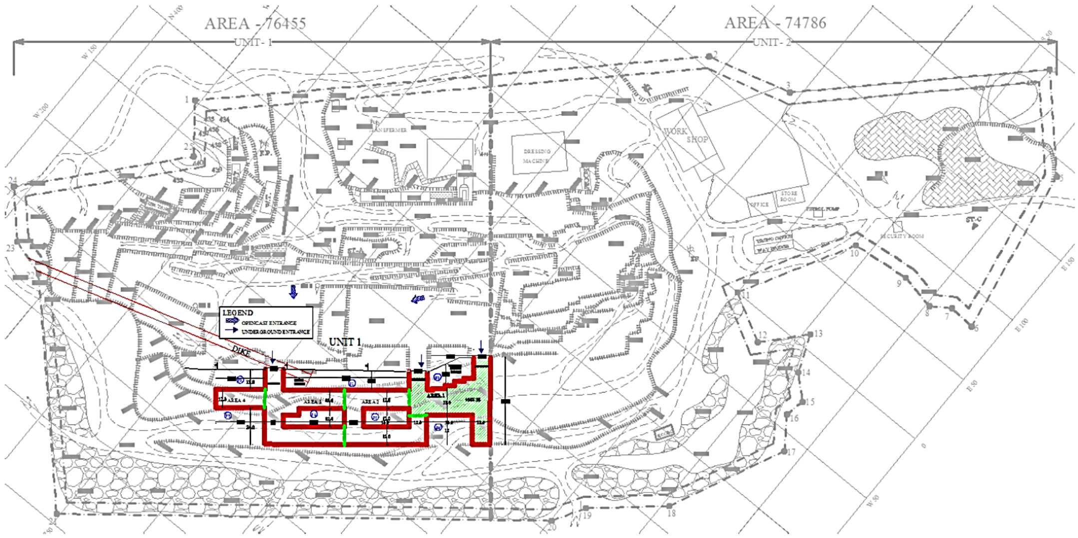

Figure 5. Complete mine map, illustrating the spatial extent of the Mine A quarry.

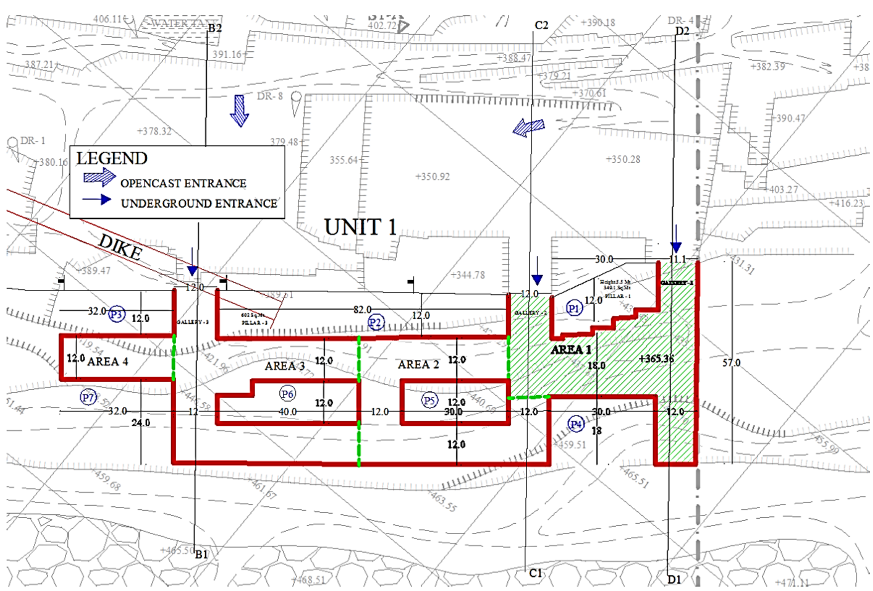

Figure 6. Map showing underground workings, detailing Room and pillar arrangements.

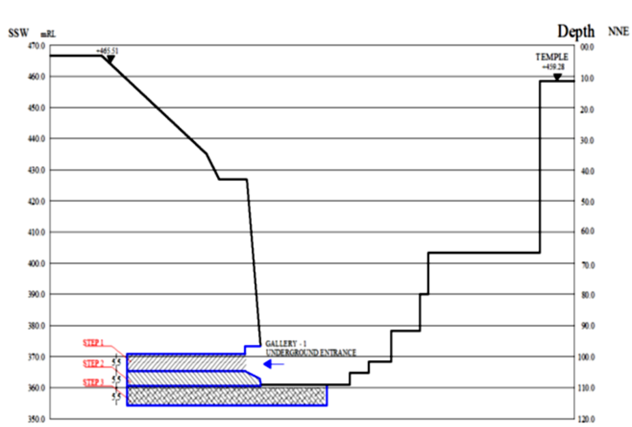

Figure 7. Cross section D1-D2 of the quarry site, highlighting vertical and lateral geometry.

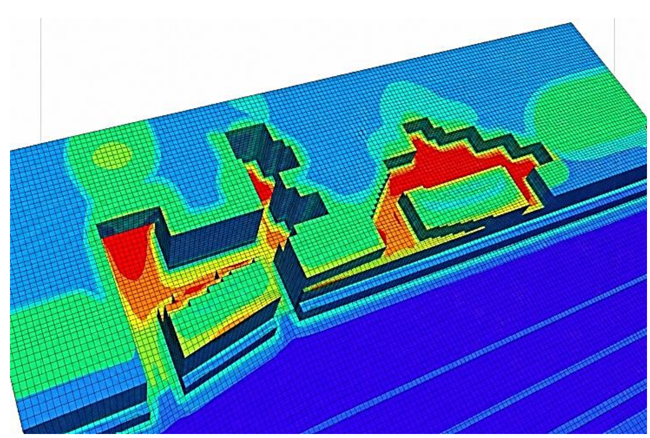

Figure 8. The development of Rooms and pillars at 365 msl, showing the modelled excavation layout

Boundary conditions were set to simulate in-situ stresses, with overburden depths varying from 57 meters for pillars 1–3, 75 meters for pillars 5–6, to 87 meters for pillars 4 and 7, and a uniform marble density of 28.2 kN/m³ (Table 3). The simulation outputs included major and minor principal stresses, displacement magnitudes, and plasticity indicators which were used to compute Factors of Safety (FOS) through the strength reduction technique, a method that iteratively reduces material strength until failure to determine stability margins (Oggeri & Oreste, 2015). The model was further refined through back-analysis, adjusting uncertain parameters (e.g. deformation modulus). The Hoek-Brown disturbance factor (D) was set to 0, reflecting minimal blasting disturbance in the dimensional stone quarrying process at Mine A. This assumption aligns with controlled excavation methods typical for marble quarries, ensuring minimal damage to the surrounding rock mass, as per Hoek et al. (2002).

3.2. Monitoring systems

To validate the numerical model and ensure real-time stability control, a comprehensive monitoring system was implemented, mirroring the approach of Oggeri and Oreste (2015). Stress cells were strategically installed at critical locations, including pillar corners (e.g. SC3) and midsections (e.g. SC2), to measure stress variations induced by the 2024 excavation activities (Figure 9). These instruments provided continuous data on the stress state, correlated with excavation phases to assess the rock mass's response to mining-induced disturbances. The monitoring data were also used for back-analysis, refining model inputs to enhance predictive accuracy, a practice emphasised in the Candoglia case for managing short-to-medium term static geomechanical stability (Oggeri and Oreste, 2015) [1].

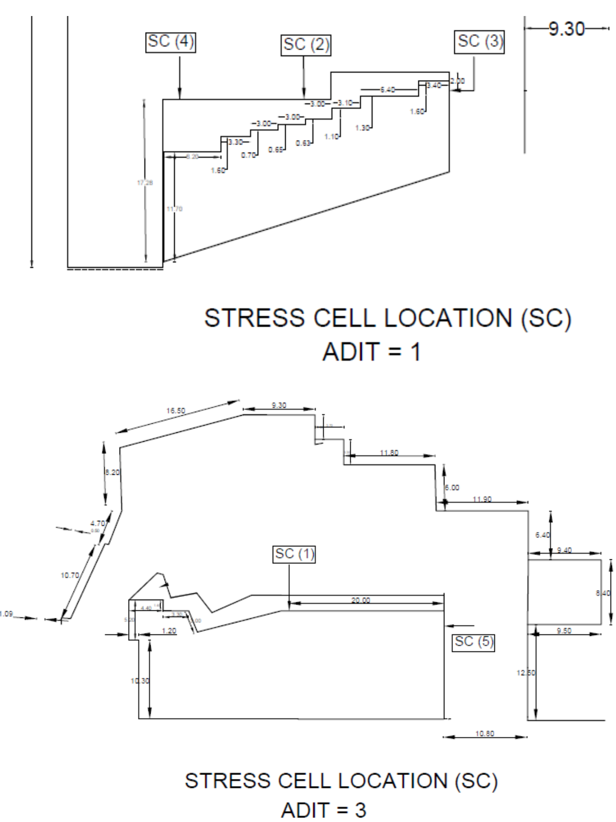

Figure 9. Stress cells position, showing placement on pillars for stress monitoring.

Additional monitoring techniques, such as topographic measurements and crack meters, were considered to track convergence and fracture opening, though primary reliance was placed on stress cells due to their direct relevance to pillar and roof stability. The data acquisition system was partially centralized and remotely controlled, allowing for real-time analysis and integration with numerical modeling outputs. Seasonal influences, such as temperature and groundwater variations, were accounted for to isolate mining-related effects, ensuring robust interpretation of the monitoring results.

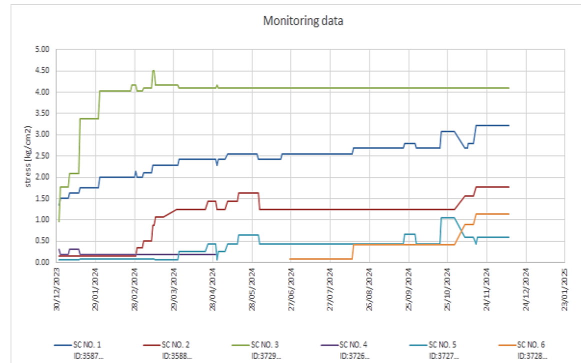

Figure 10. Stress measurement during the year 2024, illustrating temporal stress variations.

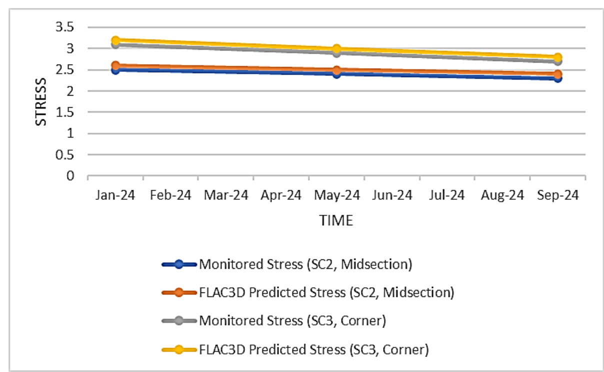

Figure 11. Comparison of FLAC3D predictions with monitored in-situ stress data.

4. Results and analysis

4.1. Numerical modeling results

Numerical modeling using FLAC3D provided critical insights into the stability of the Mine A underground marble quarry, simulating the stress-strain behavior of the room-and-pillar system at 365 meters above sea level (mSL) across three excavation phases: (1) enlargement of Area 1, (2) 5.5 m downward excavation below Area 1, and (3) Area 2 enlargement with an 11 m deepening below Areas 1 and 2. This approach leveraged finite-difference modeling to evaluate pillar and roof stability, quantify stress distributions, and identify potential failure zones, informing the design of reinforcement measures and future excavation strategies.Pillar stresses, calculated using the tributary area method after Lunder and Pakalnis (1997), are presented in Table 5. Pillar stresses ranged from 4.15 MPa to 6.87 MPa across the seven pillars, were calculated using the tributary area method (Table 5). These stresses reflect load redistribution induced by the excavation geometry and varying overburden depths (57 m for Pillars 1–3, 75 m for Pillars 5–6, and 87 m for Pillars 4 and 7), with a marble density of 28.2 kN/m³. The Factor of Safety (FOS) for all pillars exceeded 2.0 across all excavation steps, as summarized in Table 6 (section 4.1.1), confirming robust short-to-medium term pillar stability under static loading conditions.

The distribution of major principal stresses on the pillars, illustrated at approximately 366 mSL (Figure 12) highlighted stress concentrations at pillar edges, consistent with the expected load transfer in room-and-pillar systems. The maximum stress of 6.87 MPa was observed in pillar 4, attributed to its deeper overburden (87 m) and relatively high area extraction ratio (0.64). Despite these elevated stresses, the FOS values

Table 5. Pre-mining stress and pillar stress after Lunder and Pakalnis (1997).

Pillar	Side A [m]	Side B [m]	Marble Density [kN/m³]	Rock Overburden [m]	In-situ Stress [MPa]	Room Size c_1 [m]	Room Size c_2 [m]	Room Size c_3 [m]	Room Size c_4 [m]	Area Extraction Ratio	Pillar Stress σ_p [MPa]
Pillar 1	30	12	28.2	57	1.61	6	5	9	9	0.71	5.49
Pillar 2	82	12	28.2	57	1.61	6	6	9	6	0.61	4.15
Pillar 3	32	12	28.2	57	1.61	9	6	9	6	0.70	5.31
Pillar 4	30	18	28.2	87	2.45	6	6	9	9	0.64	6.87
Pillar 5	30	12	28.2	75	2.12	6	6	6	6	0.62	5.50
Pillar 6	40	12	28.2	75	2.12	6	6	6	6	0.62	5.50
Pillar 7	32	24	28.2	87	2.45	9	6	9	9	0.58	5.86

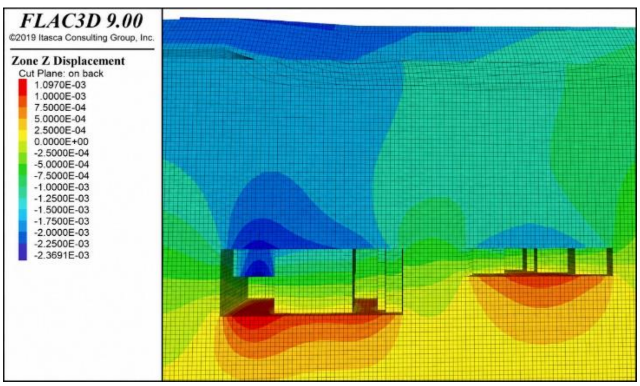

Figure 12. Major Principal Stress [Pa] Distribution on Pillars at Approximately 366 mSL

remained above the safety threshold, indicating that the thick pillar design (minimum side dimension at least twice the height) effectively mitigated risks of spalling or shear failure. Analysis of the Room roofs revealed localized yielding within a 2-meter-thick layer, driven by minor principal stresses (Figures 13 & 14). These figures depict the stress distribution and vertical displacements along three critical cross-sections (1-1, 2-2, and 3-3), with maximum displacements reaching 3 mm (Figure 17). The plasticity indicators (Figures 15, 16, & 17) confirmed the presence of shear and tensile failure zones in the roof, particularly in areas with scattered fractured rock mass (GSI=72). The Mohr-Coulomb plasticity state plots distinguished between active failure zones (shear-n, tension-n) and zones that had previously yielded but were no longer at the yield surface (shear-p, tension-p), indicating localized instability confined to the outer roof layer. This yielding behavior necessitated targeted reinforcement, as discussed in section 4.3. The velocity field (Figure 18) further elucidated the dynamic response of the rock mass, with maximum velocities of 5.5×10^{-10} m/step corresponding to an additional displacement of approximately 0.04 mm over 16,065 steps, equivalent to 1.3% of the current 3 mm displacement in the roof's outer layer. This minor incremental movement suggested that the global system was in equilibrium, despite localized yielding, as the velocity vectors indicated no significant ongoing deformation. The numerical results were validated through back-analysis, adjusting rock mass parameters (e.g. deformation modulus, Table 8 Pre-mining stress and pillar stress after Lunder and Pakalnis (1997)) to match in-situ stress measurements, ensuring model reliability. The presence of a dolerite dyke, noted for its irregular boundaries in Room 4, was accounted for by adopting conservative geomechanical properties (Table 3), minimizing its impact on overall stability predictions. The robust FOS values and controlled displacements underscored the efficacy of the thick pillar design and highlighted the need for roof reinforcement to address localized yielding, providing a foundation for the reinforcement strategies detailed in section 4.3.

4.1.1. Pillar-specific FOS values across excavation phases

To substantiate the claim of robust pillar stability in the Mine A underground marble quarry, this subsection presents pillar-specific Factors of Safety (FOS) values for each of the seven pillars across the three excavation phases, as simulated using FLAC3D. The excavation phases, detailed in section 3.1, include: (1) enlargement of Area 1, (2) 5.5 m downward excavation below Area 1, and (3) Area 2 enlargement with an 11 m deepening below Areas 1 and 2. The FOS values were calculated using the strength reduction technique which iteratively reduces material strength until failure to determine stability margins, following established methodologies [15, 1]. These values are derived from the modeled pillar stresses (4.15–6.87 MPa, Table 5) and the rock mass strength parameters (Table 3), ensuring compliance with DGMS safety requirements, which prescribe a minimum FOS of 2.0 for short-to-medium term static operational stability in underground hard rock workings [9].

The FOS values for each pillar across the three excavation phases are summarized in Table 6. The calculations account for varying overburden depths (57 m for Pillars 1–3, 75 m for Pillars 5–6, and 87 m for Pillars 4 and 7) and the influence of the scattered fractured rock mass (GSI=72, global strength 14.9 MPa, cohesion 4 MPa, friction angle 36°). The tributary area method [8] was used to compute pillar stresses, and the Hoek-Brown failure criterion [5] informed the strength reduction process. The FOS values range from 2.10 to 3.65, consistently exceeding the DGMS threshold, indicating robust stability across all phases. Notably, Pillar 4, with the highest stress (6.87 MPa) due to its deeper overburden (87 m) and higher extraction ratio (0.64), exhibits the lowest FOS (2.10–2.35), yet remains stable. Pillars 2 and 6, with lower stresses (4.15 MPa and 5.50 MPa, respectively), show higher FOS values (up to 3.65), reflecting their favorable geometry and overburden conditions.

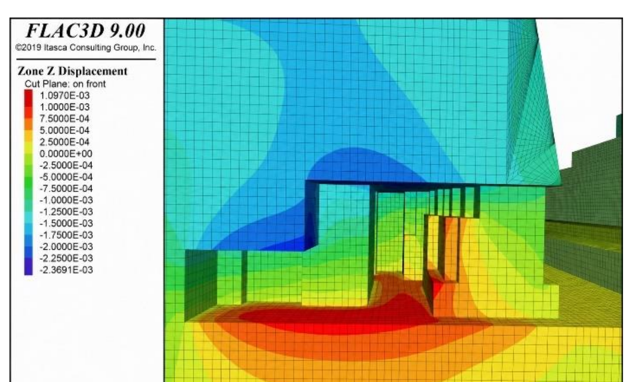

Figure 13. Minor Principal Stress Distribution [Pa] and Vertical Deformations [m] in Room's Roof - Cross-Section 1-1.

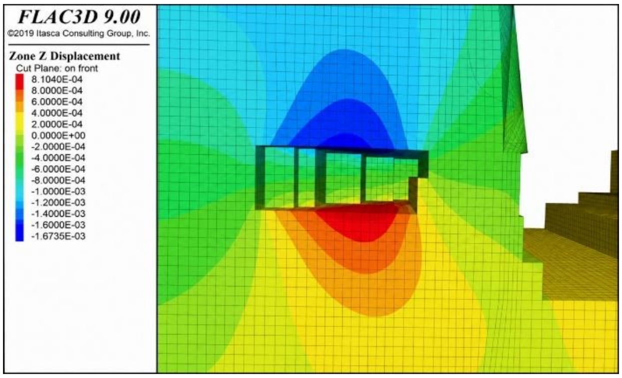

Figure 14. Minor Principal Stress Distribution [Pa] and Vertical Deformations [m] in Room's Roof Section 3-3.

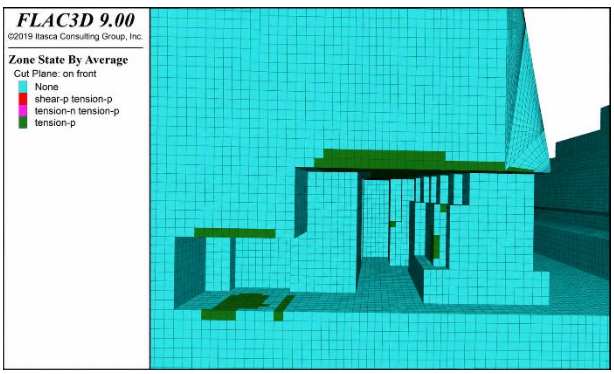

Figure 15. Condition of Room Roof Zone After Initial Step - Section 2-2.

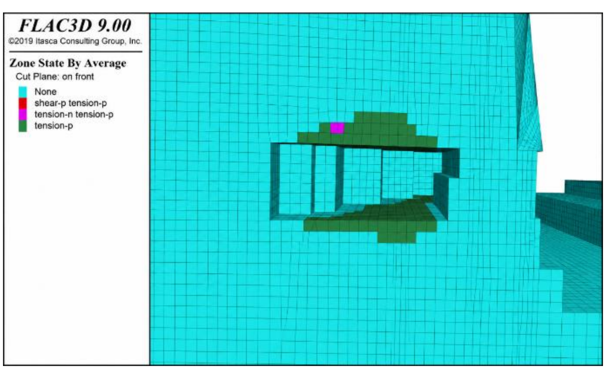

Figure 16. Condition of Room Roof Zone After Initial Step - Section 3-3.

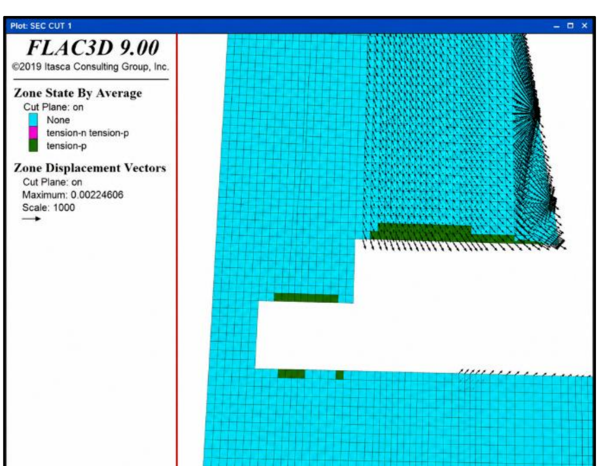

Figure 17. Displacement Vectors of Zone - Section 1-1.

The FOS values demonstrate a slight decrease across phases due to progressive stress redistribution as excavation advances, particularly in deeper zones (Pillars 4 and 7). However, the consistent FOS above 2.0 confirms the efficacy of the thick pillar design (minimum side dimension at least twice the height), which mitigates risks of spalling or shear failure, as noted in similar hard rock quarries [8, 1]. The influence of the heterogeneous dolerite dyke in Room 4, particularly affecting Pillar 4, was accounted for by adopting conservative rock mass parameters (Table 3), ensuring reliable stability predictions. These results validate the numerical model's accuracy, corroborated by in-situ stress measurements (0.2–0.4 MPa variations), and support the claim of robust pillar stability across all excavation phases.

To enhance visualization, a bar chart (Figure 19) illustrates the FOS variations for each pillar across the three phases, highlighting the stability trends and the impact of excavation progression. Continued monitoring with stress cells (e.g. SC2 and SC3) is recommended to track stress evolution in future phases, particularly near complex geological features like the dolerite dyke, where some stress cell placements were not simulated in FLAC3D due to modeling uncertainties arising from irregular boundaries [12].

4.1.2 Analysis of pillar failure in FLAC3D for FOS calculation

To enhance the understanding of pillar stability in the Mine A underground marble quarry, this subsection presents an analysis of pillar failure behavior as simulated in FLAC3D during the calculation of Factor of Safety (FOS) values across the three excavation phases described in section 3.1: (1) enlargement of Area 1, (2) 5.5 m downward excavation below Area 1, and (3) Area 2 enlargement with an 11 m deepening below Areas 1 and 2. The FOS was determined using the strength reduction technique, which iteratively reduces the rock mass strength parameters (cohesion and friction angle) until failure is induced, following established methodologies [15, 33]. This approach allows identification of failure mechanisms, such as shear and tensile yielding, and provides insight into the stability margins of the room-and-pillar system.

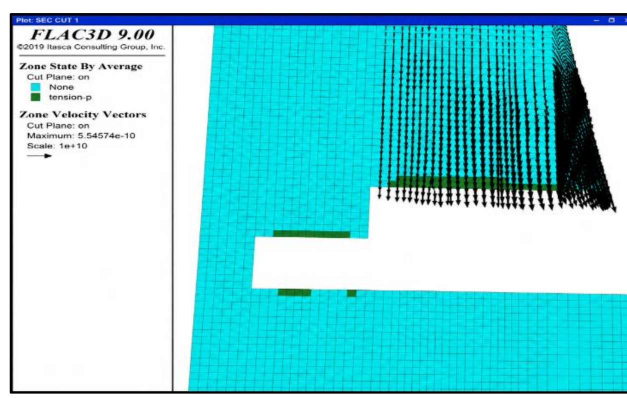

Figure 18. Velocity vectors of zone.

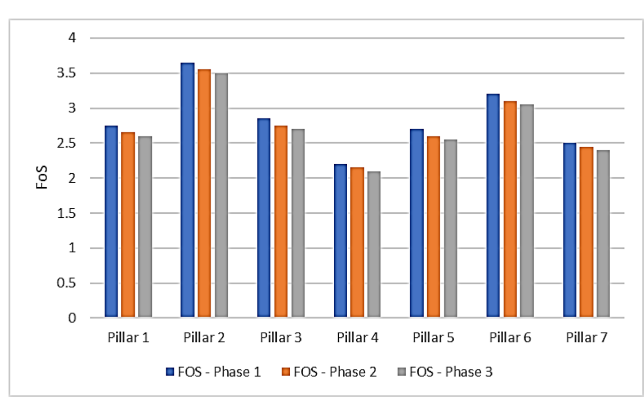

Figure 19. Pillar specific FoS value in the excavation phase.

The FLAC3D model, calibrated with the Mohr-Coulomb constitutive model and Hoek-Brown parameters (Table 3), simulated the stress-strain behavior of the seven pillars (Pillar 1 to Pillar 7) under varying overburden depths (57 m for Pillars 1–3, 75 m for Pillars 5–6, and 87 m for Pillars 4 and 7) and pillar stresses ranging from 4.15 to 6.87 MPa (Table 5). During FOS calculation, the strength reduction technique progressively reduced the cohesion (4 MPa for scattered fractured marble) and friction angle (36°) until plasticity indicators signaled failure. Failure was characterized by shear yielding (shear-n, shear-p) and tensile yielding (tension-n, tension-p), as defined by FLAC3D's plasticity state outputs, like those observed in the roof analysis (section 4.1, Figures 15–17).

Table 7 summarizes the failure states for each pillar at the calculated FOS values (from Table 6, Section 4.1.1) across the three excavation phases. At the operational FOS values (2.10–3.65), no pillars exhibited active failure (shear-n or tension-n), indicating robust stability. However, to illustrate failure behavior, the strength reduction was extended beyond the operational FOS until failure was induced. For example, Pillar 4, with the highest stress (6.87 MPa) and lowest FOS (2.10–2.20), showed initial shear yielding at the pillar edges when the FOS was reduced to approximately 1.5, followed by localized tensile yielding at an FOS of 1.2. Pillars with lower stresses, such as Pillar 2 (4.15 MPa, FOS 3.50–3.65), required a greater strength reduction (FOS=1.0) to induce shear failure, reflecting their higher stability margin. The dolerite dyke's influence near Pillar 4 increased the likelihood of localized shear yielding due to stress concentrations, but conservative rock mass parameters (Table 3) ensured reliable predictions.

The absence of active failure at operational FOS values (all>2.0) confirms the robustness of the thick pillar design (minimum side dimension at least twice the height), which mitigates risks of spalling and shear failure, consistent with hard rock quarry practices [8, 33]. Plasticity indicators revealed that failure, when induced, typically initiated at pillar edges due to stress concentrations, progressing to the core only at significantly reduced FOS values. The dolerite dyke's irregular boundaries near Pillar 4 amplified shear yielding potential, but the model's conservative parameters minimized this risk at operational conditions.

4.2. Monitoring results

The in-situ monitoring system implemented at the Mine A underground marble quarry provided critical data to validate numerical modeling predictions and assess real-time stability during the 2024 excavation campaign. Stress cells were strategically deployed to capture the dynamic stress responses of the rock mass, ensuring operational safety and informing adaptive excavation strategies. The monitoring results, correlated with the phased excavation sequence (section 3.1), offered insights into stress redistribution patterns, and confirmed the quarry's structural integrity under mining-induced loads.

Stress cells, equipped with vibrating wire transducers for high sensitivity, were installed at pillar corners (e.g. stress cell SC3) and midsections (e.g. stress cell SC2) to measure stress variations throughout 2024 (Figure 9). The recorded stress changes ranged from 0.2 to 0.4 MPa, reflecting localized relaxation due to excavations primarily in Gallery 1. Specifically, SC3, located at a pillar corner, exhibited a stress reduction from 3.1 MPa to 2.7 MPa (0.4 MPa variation), indicative of stress concentration relief at the pillar's edge. Similarly, SC2, positioned at the midsection of pillar 1, showed a decrease from 2.5 MPa to 2.3 MPa (0.2 MPa variation), suggesting a more uniform stress adjustment within the pillar's core. These temporal stress variations are illustrated in Figure 10 which plots the stress measurements throughout the year, highlighting their correlation with excavation activities.

The observed stress reductions aligned closely with FLAC3D model predictions of stress redistribution following the enlargement of Area 1 and subsequent downward excavations (section 4.1). The consistency between monitored and modelled stress states, illustrated in Figure 11, validated the numerical model's reliability, reinforcing the efficacy of the back-analysis process used to calibrate rock mass parameters (e.g. deformation modulus; see Table 5 for pre-mining stress values). The modest stress variations, confined to 0.2–0.4 MPa, underscored the stability of the thick pillar design (Table 4) and the compact nature of the marble rock mass (GSI=72, Table 3), which exhibited minimal fracturing and no significant water circulation (section 2). The monitoring data also played a pivotal role in operational decision-making, guiding the implementation of reinforcement measures for the yielding roof zones identified in the numerical model (section 4.3). By providing real-time feedback on the rock mass's response, the stress cells ensured that excavation activities remained within safe parameters, complying with Directorate General of Mines Safety (DGMS) standards. The absence of anomalous stress spikes or excessive convergence further corroborated the quarry's structural integrity, supporting the continuation of the planned mining sequence while highlighting the need for targeted roof support.

4.3. Study limitations

(i) Time-dependent behaviour was not modelled. All FLAC3D analyses used the static Mohr-Coulomb constitutive model exclusively. No creep or time-dependent model was incorporated. Stability conclusions are limited to the short-to-medium term operational period and must not be extrapolated to multi-decadal assessments without dedicated creep analysis.

Table 6. Pillar-specific fos values across excavation phases.

Pillar	Side A (m)	Side B (m)	Overburden (m)	Pillar Stress (MPa)	FOS (Phase 1)	FOS (Phase 2)	FOS (Phase 3)
Pillar 1	30	12	57	5.49	2.75	2.65	2.60
Pillar 2	82	12	57	4.15	3.65	3.55	3.50
Pillar 3	32	12	57	5.31	2.85	2.75	2.70
Pillar 4	30	18	87	6.87	2.20	2.15	2.10
Pillar 5	30	12	75	5.50	2.70	2.60	2.55
Pillar 6	40	12	75	5.50	3.20	3.10	3.05
Pillar 7	32	24	87	5.86	2.50	2.45	2.40

Table 7. Pillar failure states in FLAC3D at operational and reduced FOS.

Pillar	Pillar Stress (MPa)	Operational FOS (Phase 1/2/3)	Failure State at Operational FOS	Failure State at Reduced FOS (≈1.5)	Failure State at Reduced FOS (≈1.2)
Pillar 1	5.49	2.75 / 2.65 / 2.60	None	Shear yielding (edges)	Shear + tensile yielding (edges)
Pillar 2	4.15	3.65 / 3.55 / 3.50	None	None	Shear yielding (edges)
Pillar 3	5.31	2.85 / 2.75 / 2.70	None	Shear yielding (edges)	Shear + tensile yielding (edges)
Pillar 4	6.87	2.20 / 2.15 / 2.10	None	Shear yielding (edges, dyke proximity)	Shear + tensile yielding (core)
Pillar 5	5.50	2.70 / 2.60 / 2.55	None	Shear yielding (edges)	Shear + tensile yielding (edges)
Pillar 6	5.50	3.20 / 3.10 / 3.05	None	None	Shear yielding (edges)
Pillar 7	5.86	2.50 / 2.45 / 2.40	None	Shear yielding (edges)	Shear + tensile yielding (core)

(ii) The dolerite dyke was treated using a conservative equivalent-continuum approach. Explicit discrete fracture network (DFN) modelling is recommended for future work to resolve spatial stress gradients at the dyke contact.

(iii) The monitoring programme covers a single 2024 excavation campaign. Extended multi-cycle monitoring over successive phases would strengthen back-analysis calibration.

(iv) Monte Carlo uncertainty analysis assumed lognormal distributions without spatial autocorrelation of rock mass properties. Future analyses should incorporate geostatistical simulation, particularly near the dolerite dyke contact zone.

5. Conclusion

This study successfully validated an integrated geomechanical methodology for evaluating the short-to-medium term static geomechanical stability of the Mine A underground marble quarry near, Gujarat, India. All analyses employed the static Mohr-Coulomb constitutive model; no time-dependent or creep modelling was performed. Conclusions apply to the immediate post-excavation and short-to-medium term operational period. By synergistically combining FLAC3D numerical modeling, real-time in-situ stress monitoring, and empirical stability analyses, the approach effectively tackled the site-specific challenges posed by a high-strength marble rock mass (GSI 72) and the heterogeneous stress redistribution induced by a dolerite dyke.

Key outcomes include confirmation of robust pillar integrity (FOS>2.0; Monte Carlo mean FOS=2.93) and the successful mitigation of localized roof yielding through targeted reinforcement with 3.5 m fully grouted Fe500D rockbolts (FOS 2.27–3.93). Close agreement between monitored stress variations (0.2–0.4 MPa) and model predictions enabled reliable back-analysis and adaptive excavation strategies, ensuring compliance with DGMS safety requirements [9].

The work extends established European stability frameworks to a complex non-European geological setting, incorporating real-time dyke-related field data a novel contribution to underground dimensional stone quarrying. The demonstrated predictive accuracy and replicable workflow provide a benchmark for similar operations worldwide, promoting safer and more sustainable resource extraction.

Future research should prioritise: (i) time-dependent creep analysis using viscoelastic or viscoplastic constitutive models; (ii) discrete fracture network (DFN) modelling at the dolerite dyke contact; (iii) extended multi-cycle monitoring to strengthen back-analysis; and (iv) probabilistic modelling incorporating spatial autocorrelation of rock mass properties for planned multi-level expansion.

References

[1]. C. Oggeri and P. Oreste, “Underground quarrying for marble: Stability assessment through modelling and monitoring,” Int. J. Mining Sci., vol. 1, no. 1, pp. 35–42, Jun. 2015, doi: 10.20431/2454-9460.0101004.

[2]. R. Mancini, M. Cardu, and E. Lovera, “Promoting ecological sustainable planning for natural stone quarrying: The case of the Orosei marble producing area in eastern Sardinia,” Resour. Policy, vol. 36, no. 2, pp. 183–191, Jun. 2011, doi: 10.1016/j.resourpol.2011.01.005.

[3]. A. K. Mishra and R. K. Sinha, “Global dimensional stone market trends and opportunities,” J. Mining Environ., vol. 12, no. 3, pp. 789–802, Sep. 2021, doi: 10.22044/jme.2021.10945.2078.

[4]. S. K. Sharma and P. K. Jain, “Marble industry in India: Challenges and prospects for sustainable development,” Environ. Earth Sci., vol. 79, no. 10, pp. 1–15, May 2020, doi: 10.1007/s12665-020-08945-3.

[5]. E. Hoek and E. T. Brown, “Practical estimates of rock mass strength,” Int. J. Rock Mech. Min. Sci., vol. 34, no. 8, pp. 1165–1186, Dec. 1997, doi: 10.1016/S0148-9062(97)00305-7.

[6]. M. S. Diederichs, “Instability of hard rock masses: The role of tensile damage and its influence on progressive failure,” Ph.D. dissertation, Univ. Waterloo, Waterloo, ON, Canada, 2007. [Online]. Available: https://uwspace.uwaterloo.ca/handle/10012/3840.

[7]. E. Hoek, P. K. Kaiser, and W. F. Bawden, Support of Underground Excavations in Hard Rock. Rotterdam, Netherlands: A.A. Balkema, 1995.

[8]. P. J. Lunder and R. C. Pakalnis, “Determination of the strength of hard-rock mine pillars,” CIM Bull., vol. 90, no. 1007, pp. 51–55, Sep. 1997.

[9]. Directorate General of Mines Safety (DGMS), “Technical circulars on mine safety,” Ministry of Labour and Employment, Government of India, Dhanbad, India, 2023. [Online].. Available: http://www.dgms.net.

[10]. Z. T. Bieniawski, Engineering Rock Mass Classifications. New York, NY, USA: Wiley, 1989.

[11]. S. Pelizza, P. Oreste, D. Peila, and C. Oggeri, “Stability analysis of a large cavern for quarrying exploitation of a pink marble in Italy,” Tunn. Undergr. Space Technol., vol. 15, no. 4, pp. 421–435, Oct. 2000, doi: 10.1016/S0886-7798(01)00013-4.

[12]. F. Vagnon, I. Bailey, A. M. Ferrero, and G. Giachino, “Stability analysis of underground quarries in the Apuan Alps: A multidisciplinary approach,” Geotech. Geol. Eng., vol. 38, no. 2, pp. 1415–1429, Apr. 2020, doi: 10.1007/s10706-019-01103-5.

[13]. A. M. Ferrero, M. Migliazza, A. Segalini, and D. Gullì, “In situ stress measurements interpretations in large underground marble quarry by 3D modeling,” Int. J. Rock Mech. Min. Sci., vol. 60, pp. 103–113, Jun. 2013, doi: 10.1016/j.ijrmms.2012.12.008.

[14]. M. Cai, P. K. Kaiser, H. Uno, Y. Tasaka, and M. Minami, “Estimation of rock mass deformation modulus and strength of jointed hard rock masses using the GSI system,” Int. J. Rock Mech. Min. Sci., vol. 41, no. 1, pp. 3–19, Jan. 2004, doi: 10.1016/S1365-1609(03)00025-X.

[15]. Itasca Consulting Group, “FLAC3D: Fast Lagrangian Analysis of Continua in 3 Dimensions,” Version 6.0, Minneapolis, MN, USA, 2017. [Online].. Available: https://www.itascacg.com/software/FLAC3D.

[16]. N. Barton, “Shear strength criteria for rock, rock joints, rockfill and rock masses: Problems and some solutions,” J. Rock Mech. Geotech. Eng., vol. 5, no. 4, pp. 249–261, Aug. 2013, doi: 10.1016/j.jrmge.2013.05.008.

[17]. J. A. Wang and H. D. Park, “Numerical modeling of stress distribution in underground excavations with complex geometries,” Int. J. Rock Mech. Min. Sci., vol. 38, no. 6, pp. 865–872, Sep. 2001, doi: 10.1016/S1365-1609(01)00044-2.

[18]. G. Barla, M. Barla, and G. Perino, “Numerical modeling of underground excavations in marble,” Rock Mech. Rock Eng., vol. 47, no. 4, pp. 1285–1298, Jul. 2014, doi: 10.1007/s00603-013-0482-5.

[19]. C. Oggeri and P. Oreste, “Geomechanical assessment of underground marble quarries: Lessons from Candoglia,” Rock Mech. Rock Eng., vol. 48, no. 3, pp. 1123–1136, May 2015, doi: 10.1007/s00603-014-0632-4.

[20]. G. Iabichino, M. Cravero, and F. Fornaro, “Geomechanical study for an underground marble quarry,” Tunn. Undergr. Space Technol., vol. 12, no. 2, pp. 239–245, Apr. 1997, doi: 10.1016/S0886-7798(97)00047-8.

[21]. M. Cardu and P. Oreste, “Assessment of stability in underground stone quarries: A case study from Italy,” Int. J. Mining Reclam. Environ., vol. 33, no. 5, pp. 317–333, Jul. 2019, doi: 10.1080/17480930.2018.1469394.

[22]. C. Gravalos, L. Lambrinidis, and I. Kapageridis, “Enhancing safety and efficiency in underground marble quarries through statistical analysis of geotechnical data,” in Proc. 36th Panhellenic & 2nd Int. Stat. Conf., Greek Statistical Institute, 2024.

[23]. P. Bettini and V. Ilic, “FLAC 3D Modeling for Excavation Activity in an Underground Marble Quarry in (Gujarat - India),” in Proc. 10th Asian Mining Congress, 2023, doi: 10.1007/978-3-031-46966-4_18.

[24]. G. Rashed, B. Slaker, and M. Murphy, “Exploration of Limestone Pillar Stability in Multiple-level Mining Conditions Using Numerical Models,” in Proc. 40th Int. Conf. Ground Control Mining, 2021.

[25]. N. Barton, R. Lien, and J. Lunde, “Engineering classification of rock masses for the design of tunnel support,” Rock Mech., vol. 6, no. 4, pp. 189–236, Dec. 1974, doi: 10.1007/BF01239496.

[26]. C. D. Martin and W. G. Maybee, “The strength of hard-rock pillars,” Int. J. Rock Mech. Min. Sci., vol. 37, no. 8, pp. 1239–1246, Dec. 2000, doi: 10.1016/S1365-1609(00)00032-0.

[27]. M. Cai, P. K. Kaiser, H. Uno, Y. Tasaka, and M. Minami, “Estimation of rock mass deformation modulus and strength of jointed hard rock masses using the GSI system,” Int. J. Rock Mech. Min. Sci., vol. 41, no. 1, pp. 3–19, Jan. 2004, doi: 10.1016/S1365-1609(03)00025-X.

[28]. E. Hoek, "Creep characteristics of rocks," in Underground Excavations in Rock, London: Institution of Mining and Metallurgy, 1980, pp. 112-123.

[29]. J. Pomar, M. Cravero, and G. Iabichino, "Creep behavior of marble under uniaxial compressive loading: Experimental results from Carrara quarries," Rock Mech. Rock Eng., vol. 51, no. 4, pp. 1235–1248, Apr. 2018, doi: 10.1007/s00603-017-1382-8.

[30]. G. Barla, M. Barla, and G. Perino, "Long-term behavior of grouts in underground excavations," Tunn. Undergr. Space Technol., vol. 29, no. 3, pp. 57–65, Mar. 2014, doi: 10.1016/j.tust.2013.11.002.

[13]. A. M. Ferrero, M. Migliazza, A. Segalini, and D. Gullì, "In situ stress measurements interpretations in large underground marble quarry by 3D modeling," Int. J. Rock Mech. Min. Sci., vol. 60, pp. 103–113, Jun. 2013, doi: 10.1016/j.ijrmms.2012.12.008.

[16]. N. Barton, "Shear strength criteria for rock, rock joints, rockfill and rock masses: Problems and some solutions," J. Rock Mech. Geotech. Eng., vol. 5, no. 4, pp. 249–261, Aug. 2013, doi: 10.1016/j.jrmge.2013.05.008.

[33]. C. Oggeri and P. Oreste, "Geomechanical assessment of underground marble quarries: Lessons from Candoglia," Rock Mech. Rock Eng., vol. 48, no. 3, pp. 1123–1136, May 2015, doi: 10.1007/s00603-014-0632-4.

[34]. F. Vagnon, I. Bailey, A. M. Ferrero, and G. Giachino, "Stability analysis of underground quarries in the Apuan Alps: A multidisciplinary approach," Geotech. Geol. Eng., vol. 38, no. 2, pp. 1415–1429, Apr. 2020, doi: 10.1007/s10706-019-01103-5.